Earthquake Engineering & Structural Dynamics

WILEY

RESEARCH ARTICLE

Shake Table Testing Methodology for Multistory Floor Acceleration Simulation Using a Single-Story Test Specimen

Chao-Hsien Li[1] | Chia-Ming Uang[2] | Robert B. Fleischman[3]

[1]CoreBrace, LLC, West Jordan, Utah, USA | [2]Department of Structural Engineering, University of California San Diego, La Jolla, California, USA | [3]Department of Civil and Architectural Engineering and Mechanics, University of Arizona, Tucson, Arizona, USA

Correspondence: Chao-Hsien Li (chl228@eng.ucsd.edu)

Received: 21 May 2024 | **Revised:** 13 February 2025 | **Accepted:** 20 February 2025

Funding: This research was supported by the National Science Foundation (NSF), Engineering for Natural Hazards (ENH) program under Grant CMMI-1662816 and Supplement CMMI-1937703.

Keywords: earthquake engineering | floor acceleration | large-scale structural testing | shake table testing | structural dynamics

ABSTRACT

This study integrates analytical and experimental research to develop an innovative shake table testing method called Floor Acceleration Simulation Test (FAST). The primary objective of FAST is to produce an essentially elastic response of a single-story test specimen to replicate the floor acceleration time history including higher-mode effects of a target floor in a multistory building experiencing inelastic behavior during an earthquake. The FAST method is well suited for experimental research where the absolute accelerations and the associated inertial forces of the floor diaphragms cannot be simulated by the majority of the conventional test methods. The proposed methodology is based on a transfer function in the frequency domain to compute the required input motion for testing. Considering the physical constraints of a given shake table test facility, guidelines with two response spectra to bracket the natural frequency of the test building are also presented for practical implementation. Experimental validation was carried out on a half-scale, single-story steel building featuring a composite floor slab, utilizing the NHERI@UCSD Large High-Performance Outdoor Shake Table (LHPOST) facility. The results demonstrate the effectiveness of FAST, as both analytical predictions and experimental outcomes confirm its validity. Despite instances of measured floor acceleration amplitude exceeding the target response due to table input motion overshooting in this test program, test results confirmed that the FAST accurately reproduced the intended frequency content, indicative of higher mode effects in the multistory prototype building, in the single-story test building.

1 | Introduction

Over the last three decades, the majority of research in earthquake engineering for building structures has been centered around the vertical-plane seismic force-resisting system (SFRS). Only in recent years have several researchers [1–3] begun to focus on topics related to the seismic behavior of floor diaphragms. Motivated by the collapse of the CTV building [4] during the 2011 Christchurch earthquake due to inadequate collectors in the floor diaphragms, a collaborative program involving the University of Arizona (UA), the University of California San Diego (UCSD), and Lehigh University (LU) has been underway since 2017. This program integrates analytical and experimental research on the seismic behavior of collectors in steel building structures [5].

One of the primary objectives of this program is to investigate the response of steel collectors under inertial force mechanisms in the floor diaphragm. To conduct an experimental study on this

topic, shake table testing on a multistory test building is ideal, as it allows for the simulation of realistic inertial force mechanisms including higher-mode effects in the laboratory. However, conducting shake table testing on a relatively large-scale multistory test building comes with challenges due to high costs, extensive time requirements, and limited facility availability. In addition, although some hybrid simulation testing approaches like pseudo-dynamic testing or analysis-driven testing [6] can subject floor diaphragm specimens as a substructure from a prototype building to simulated seismic displacement loading histories, these test methods cannot produce realistic inertial forces as the acceleration response is not simulated. Further, the University at Buffalo Nonstructural Component Simulator (UB-NCS) technique [7, 8] is capable of simultaneously imposing the floor accelerations and inter-story drifts on nonstructural components attached to the floor, nonetheless, it requires a special mechanism between the testing frame and actuators and the test frame with pin-ended columns cannot represent the realistic interaction between the floor diaphragms and vertical-plane SFRS. Moreover, the substructural shake table testing with real-time hybrid simulation technology may provide a solution to test a floor diaphragm with realistic inertial forces, however, the progress of this technique is still in the preliminary stage. Hence, there is a need to develop a simple testing method to facilitate the research on the seismic response of floor diaphragm systems under inertial force mechanism.

As part of a collaborative research effort among three universities, this study aims to develop an innovative Floor Acceleration Simulation Test (FAST) methodology. FAST enables a single-story test specimen of a reasonable size to replicate the floor acceleration history response from any floor in a prototype multistory building with an approximate adjustment for story drifts, thereby enhancing the efficiency of shake table testing for evaluating the seismic performance of structural elements (such as collectors, chords, and floor diaphragms) whose seismic demand is mainly driven by the floor accelerations of building structures and, to a less extent, driven by the interstory drift.

Before the theoretical development and the associated experimental verification are presented, an overview of the concepts follows. Figure 1 illustrates the concept of the FAST methodology. Initially, a prototype multistory building is selected, and one of its seismic floor acceleration history responses is chosen as the target response for the test specimen (see Figure 1a). The chosen target acceleration response, denoted as $\ddot{u}_i^t$ for the absolute (i.e., total) acceleration of the i-th floor, can be obtained through a nonlinear response history analysis (NLRHA) on a building model subjected to a ground motion input, $\ddot{u}_g$. Subsequently, as depicted in Figure 1b, the test specimen is designed as a single-story building comprising a vertical SFRS (V-SFRS), multiple gravity columns, and a floor diaphragm. In the specimen, the floor diaphragm and its components such as collectors are the primary subjects of the research, while the V-SFRS functions as an elastic force-restoring system and serves as a vehicle governing the sway motion of the specimen such that the floor acceleration, $\ddot{u}^{t*}$, replicates the target response $\ddot{u}_i^t$ in a shake table test. The V-SFRS of the specimen is intended to remain elastic for two reasons: (1) the elasticity allows for the development of a transfer function approach to derive the required shake table input acceleration, $\ddot{u}_g^*$, and (2) the specimen can be used for multiple tests, e.g., the specimen can be first used to investigate the diaphragm system (including collectors) of a particular floor in the prototype building experiencing inelastic actions, and then it can be reused for a subsequent test to study another floor by changing the table input motion, $\ddot{u}_g^*$.

This paper first introduces the derivation of a transfer function for computing the required input motions for the proposed FAST methodology, followed by numerical verification through a case study and a discussion of appropriate single-story test specimen configurations. Recommendations are made for developing response spectra for the input table acceleration and the specimen displacement, which help bracket the natural frequency of the test specimen. Lastly, experimental validation with a half-scale single-story steel test building is presented.

2 | Transfer Function for Computing the Required Input Motion

The FAST methodology conceptualizes the specimen as an idealized elastic single-degree-of-freedom (SDOF) system. Figure 2a depicts the model of this system subjected to an input ground acceleration $\ddot{u}_g^*(t)$, with the resulting floor acceleration response history matches that of the i-th floor in the prototype building. The equation of motion for this system is shown as follows:

$$m\ddot{u}^*(t) + c\dot{u}^*(t) + ku^*(t) = -m\ddot{u}_g^*(t) \tag{1}$$

In the equation, m, c, and k represent the mass, damping coefficient, and stiffness, respectively. Additionally, $\ddot{u}^*$, $\dot{u}^*$, and u^* denote the relative acceleration, velocity, and displacement, respectively. It is important to note that the superscript "*" is utilized to signify that these responses are associated with the one-story test specimen, not the responses of the prototype structure. Likewise, $\ddot{u}_g^*$ refers to the table motion input for the test specimen, not a ground motion for the prototype structure. Furthermore, Equation (1) can be reformulated as [9]:

$$\ddot{u}^*(t) + 2\xi^*\omega_n^*\dot{u}^*(t) + {\omega_n^*}^2u^*(t) = -\ddot{u}_g^*(t) \tag{2}$$

where ω_n^* and ξ^* are the natural angular frequency and damping ratio of the SDOF system, respectively. By taking a Fourier transform of Equation (2) and considering the relations $\dot{u}^*(\omega) = i\omega u^*(\omega)$ and $\ddot{u}^*(\omega) = -\omega^2 u^*(\omega)$, the equation of motion can be expressed as:

$$-\omega^2 u^*(\omega) + i2\xi^*\omega_n^*\omega u^*(\omega) + {\omega_n^*}^2u^*(\omega) = -\ddot{u}_g^*(\omega) \tag{3}$$

This equation establishes the relationship between $u^*(\omega)$ and $\ddot{u}_g^*(\omega)$, enabling the derivation of the transfer function, $H_0(\omega)$, for an SDOF system in the frequency domain as follows:

$$H_0(\omega) = \frac{u^*(\omega)}{\ddot{u}_g^*(\omega)} = \frac{1}{\omega^2 - i2\xi^*\omega_n^*\omega - {\omega_n^*}^2} \tag{4}$$

For research on the response of floor diaphragm systems and the associated structural components, it is the absolute acceleration, $\ddot{u}^{t*}$, not the relative acceleration, $\ddot{u}^*$, that is of importance in the determination of the inertial forces (see Figure 2b). The time

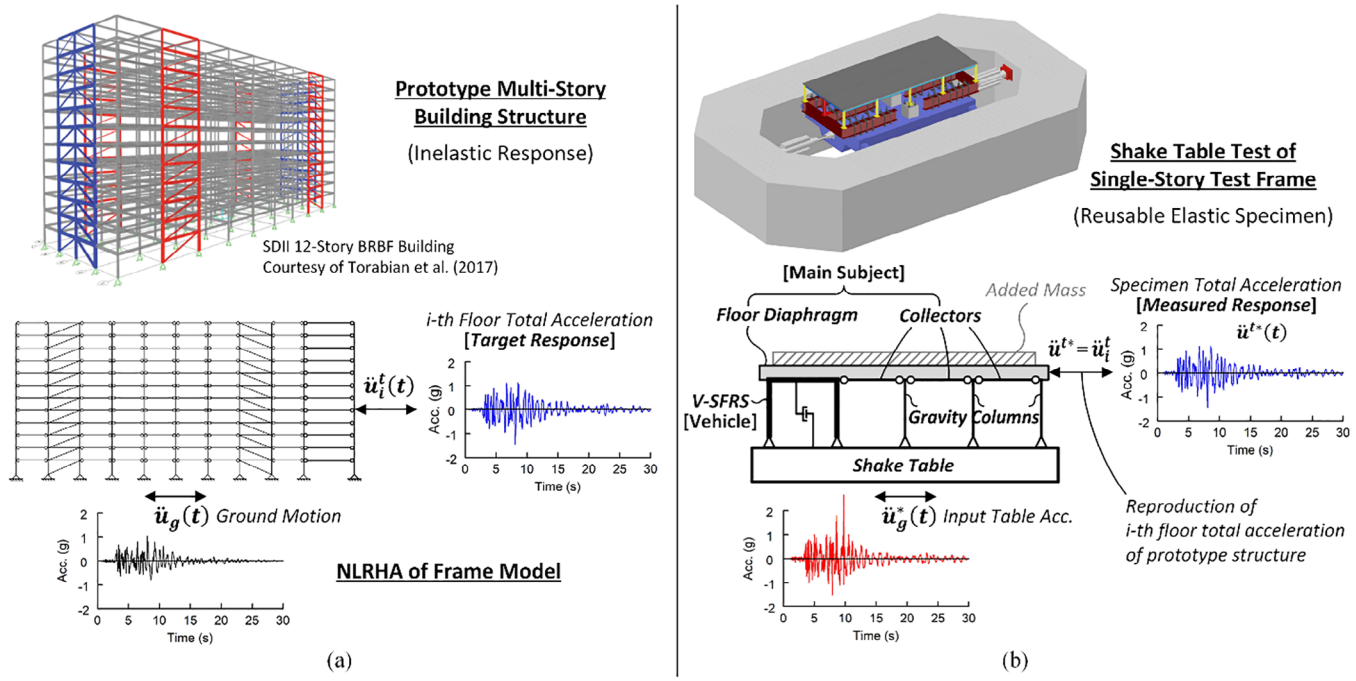

FIGURE 1 | Concept of floor acceleration simulation test: (a) prototype multistory building structure and (b) single-story test specimen.

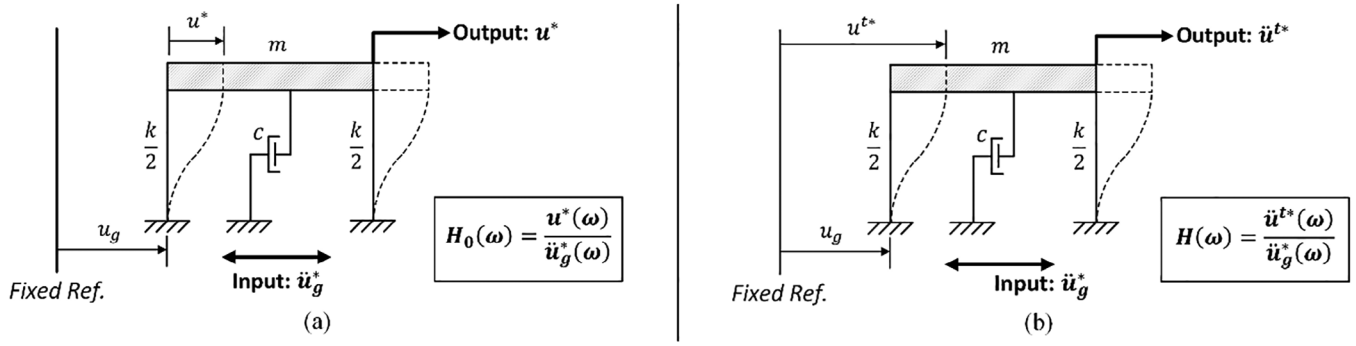

FIGURE 2 | SDOF systems with output as (a) relative displacement (u^*) and (b) absolute acceleration ($\ddot{u}^{t*}$).

history of absolute acceleration can be expressed as:

$$\ddot{u}^{t*}(t) = \ddot{u}^*(t) + \ddot{u}_g^*(t) \tag{5}$$

Performing a Fourier transform on Equation (5) results in the following:

$$\begin{aligned}\ddot{u}^{t*}(\omega) &= \ddot{u}^*(\omega) + \ddot{u}_g^*(\omega) = -\omega^2 u^*(\omega) + \ddot{u}_g^*(\omega) \\ &= -\omega^2 H_0(\omega)\ddot{u}_g^*(\omega) + \ddot{u}_g^*(\omega) = \left[1 - \omega^2 H_0(\omega)\right]\ddot{u}_g^*(\omega)\end{aligned} \tag{6}$$

The corresponding transfer function $H(\omega)$ then can be established as follows:

$$H(\omega) = \frac{\ddot{u}^{t*}(\omega)}{\ddot{u}_g^*(\omega)} = \left[1 - \omega^2 H_0(\omega)\right] = \frac{i2\xi^*\omega_n^*\omega + \omega_n^{*2}}{-\omega^2 + i2\xi^*\omega_n^*\omega + \omega_n^{*2}} \tag{7}$$

With this transfer function, solving the inverse problem to determine the required input motion, $\ddot{u}_g^*(t)$, for an SDOF system (i.e., a single-story test specimen) to replicate the target absolute acceleration time history, $\ddot{u}_{TGT}^t(t)$, becomes straightforward, in contrast to the computational complexity of doing so in the time domain. For actual implementation in testing, equate $\ddot{u}_{TGT}^t(\omega)$ to $\ddot{u}_i^t(\omega)$, the latter representing the absolute acceleration of the i-th floor in the prototype building expressed in the frequency domain. The required input motion for the shake table testing in the frequency domain can be computed as:

$$\ddot{u}_g^*(\omega) = \frac{\ddot{u}_{TGT}^t(\omega)}{H(\omega)} \tag{8}$$

An inverse FFT of $\ddot{u}_g^*(\omega)$ is then executed to obtain the required input motion, $\ddot{u}_g^*(t)$, for testing. It is worth noting that, in this transfer function approach, the dynamic structural characteristics (ω_n^* and ξ^*) of the one-story test specimen are independent of those of the prototype structure. That is, the single-story test building usually will not be a substructure or a scaled model of the multistory prototype building.

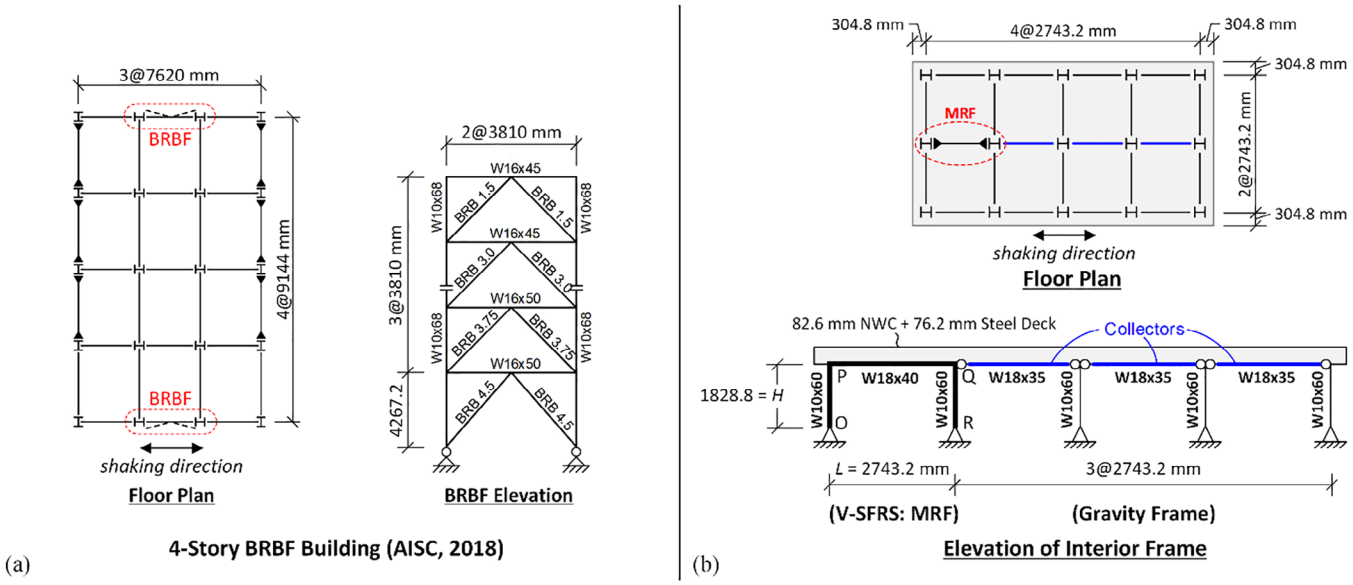

FIGURE 3 | Example structures for numerical verification: (a) prototype building (b) test building.

3 | Numerical Verification: A Case Study

This section presents a case study using numerical simulation. Configurations of single-story test specimens appropriate for applying the FAST method are also explored. It is assumed in this numerical simulation that the input motion can be faithfully imparted to the base of the single-story specimen model. The effect of the fidelity of input motion in actual shake table testing will be evaluated in the experimental verification section. Figure 3a,b depict a four-story prototype building and a single-story test building, respectively, for the application of the FAST methodology. In Figure 3a, the prototype building is taken from the AISC Seismic Design Manual [10]. The building features a single-bay buckling-restrained braced frame (BRBF) serving as the primary V-SFRS on each side of the perimeter in the short direction. Figure 3b depicts a single-story building with plan dimensions sized to fit a large size shake table. It features a one-bay, pin-based steel moment resisting frame (MRF), 13 gravity system columns, and composite beams with a concrete-filled metal deck floor. The long direction of the test building corresponds to the direction of shaking.

Figure 4 shows two finite element models created in the nonlinear structural analysis software PISA3D [11]. A two-dimensional (2-D) nonlinear frame model, depicted in Figure 4a, comprises a braced frame and a leaning column interconnected with pin-ended rigid links. The elastic leaning column represents the gravity columns of half of the prototype building. The buckling-restrained braces were modeled using truss elements with a material model employing a two-surface plastic hardening rule [12] that simulates the brace responses reported in ref. [13], while beams and columns in the braced frame were modeled using lumped plasticity beam elements with a bilinear material model having a yield stress of 55 ksi and a post-yield stiffness that equals 2% of the initial stiffness. This model has a fundamental period $T_1 = 0.819$ s with a 2% Rayleigh damping ratio for the 1st and 2nd modes. An NLRHA was conducted using a ground motion recorded in the 1994 Northridge earthquake ('Vasquez Rock Park' Station), scaled to the maximum considered earthquake (MCE) level at period T_1. The recorded ground motion was scaled to the MCE level with $S_{DS} = 1.0$ and $S_{D1} = 0.6$ [14]. Figure 5a shows the computed total acceleration time history of the 3rd floor, $\ddot{u}_3^t(t)$. This response history was chosen as the target response for the single-story test building.

In Figure 4b, a 2-D elastic frame model is used to model the entire test building. The pin-based MRF (O-P-Q-R) serves as the elastic V-SFRS. Note that the collectors are assumed to be pin-ended in the analytical models in this research. Based on the selected member sizes used and the reactive weight, the fundamental period of this model is $T_n^* = 0.19$ s ($\omega_n^* = 33.07$ rad/s). Rayleigh damping with a damping ratio of 2% was assigned to the 1st and 2nd modes of vibration. Given values of ω_n^* and ξ^*, the transfer function $H(\omega)$ for the model was calculated from Equation (7). By setting the target floor absolute acceleration response $\ddot{u}_{TGT}^t(t) = \ddot{u}_3^t(t)$, the required input motion time history, $\ddot{u}_g^*(t)$, was calculated by performing an inverse FFT of its frequency-domain counterpart, $\ddot{u}_g^*(\omega)$, from Equation (8). To confirm that the input motion thus computed can reproduce $\ddot{u}_3^t(t)$, an elastic time history analysis with $\ddot{u}_g^*(t)$ as the input motion was conducted on the test building model. Figure 5 demonstrates that the floor absolute acceleration of the test building model, $\ddot{u}^{t*}(t)$, matches very well the target response, $\ddot{u}_3^t(t)$.

In steel construction, a diaphragm is composed of not only the deck (either bare steel deck or composite slab) but also chords, collectors, and connections between the diaphragm and the members in the vertical plane of the building. Taking the collectors for example, these members not only have to carry gravity loads but also transmit floor inertial forces to the V-SFRS. Since these members are connected to either the exterior columns of the V-SFRS or gravity columns, their connections are also subjected to rotations associated with the story drift angles of the V-SFRS. Although the reproduction of target floor absolute acceleration responses is the primary focus of the FAST methodology, the accompanying story drift-related deformations

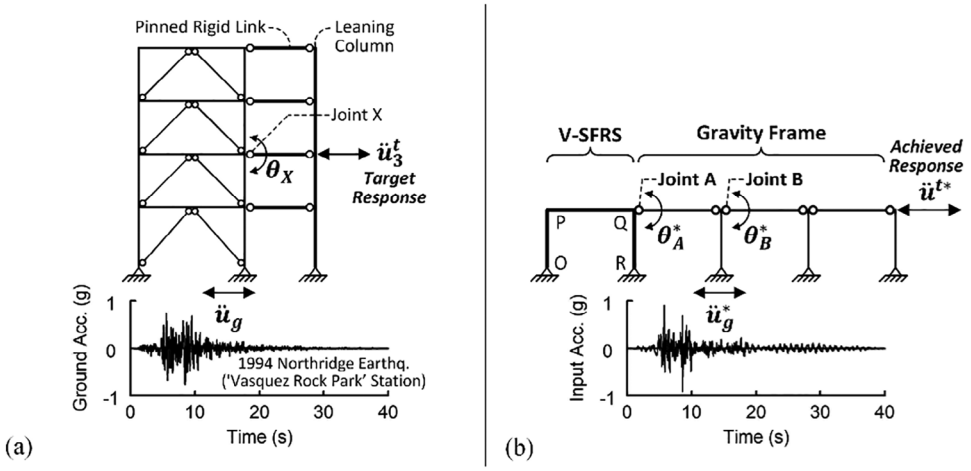

FIGURE 4 | Analytical models for (a) prototype building and (b) test building.

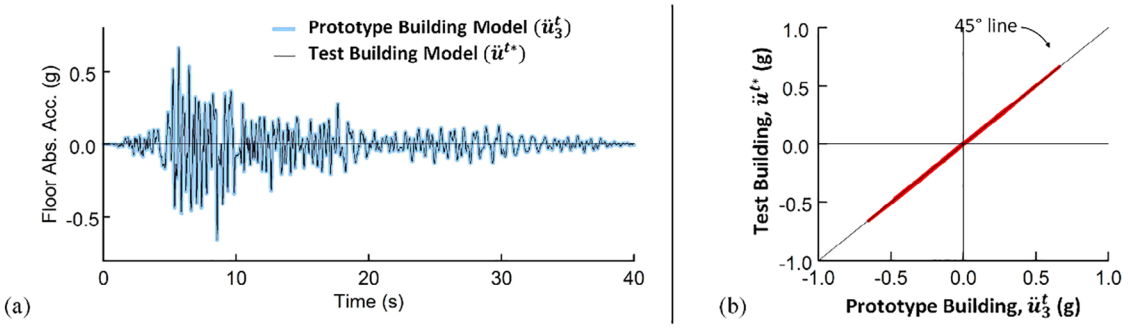

FIGURE 5 | Floor absolute accelerations time histories from prototype ($\ddot{u}_3^t$) and test ($\ddot{u}^{t*}$) building models and (b) $\ddot{u}^{t*}$ versus $\ddot{u}_3^t$ relationship.

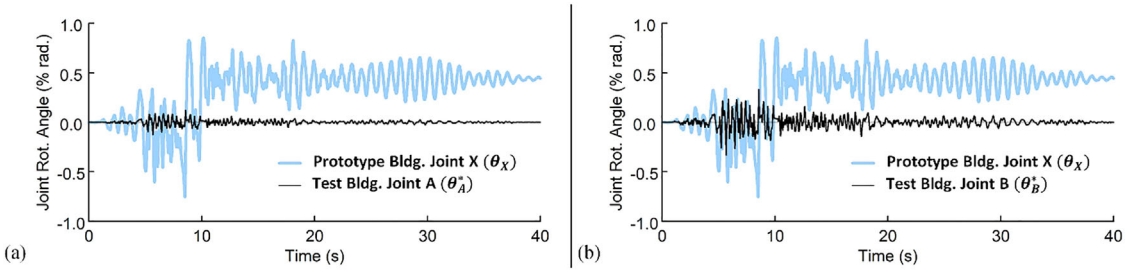

FIGURE 6 | Comparison of collector joint rotation time histories between prototype and test building models: (a) θ_X versus θ_A^* and (b) θ_X versus θ_B^*.

are also important for collector research and are thus presented next.

Referring to the same four-story prototype building in Figure 4a, the member end rotation (θ_X) time history of the 3rd-floor collector is presented in both sub-figures of Figure 6. The residual drift causes an offset joint rotation of about 0.5% rad. The corresponding response at joint A (θ_A^*) of the test building is presented in Figure 6a. Since the V-SFRS of the test building only serves as a vehicle to reproduce the target floor acceleration, the resulting joint response is not only too small but also shows no permanent offset because the test building is an elastic system. Figure 6b shows that, compared to joint A, the rotation response at joint B (θ_B^*) is larger because the gravity column to which it is connected is not subjected to bending under the sway action of the building. In such case, rotation at joint B equals to the story drift angle of the test building.

Although the FAST methodology cannot and is not intended to simulate the story drift time history response, measures can be made in actual implementation to increase the deformation amplitudes to be similar to those in the prototype building. One approach to "amplify" the story drift of the gravity columns in the test building is to shorten the length of gravity columns from H and $\tilde{H}$ as illustrated by the trial test building in Figure 7a and its analytical model in Figure 7b. Although the intended elastic response of the V-SFRS results in a small amount of story drift response (θ^*) in the V-SFRS, the story drift angle of the gravity frame, $\widetilde{\theta}^*$, is amplified by a ratio of $H/\tilde{H}$, as illustrated in Figure 7c. Since the collectors are assumed to be pin-ended, the

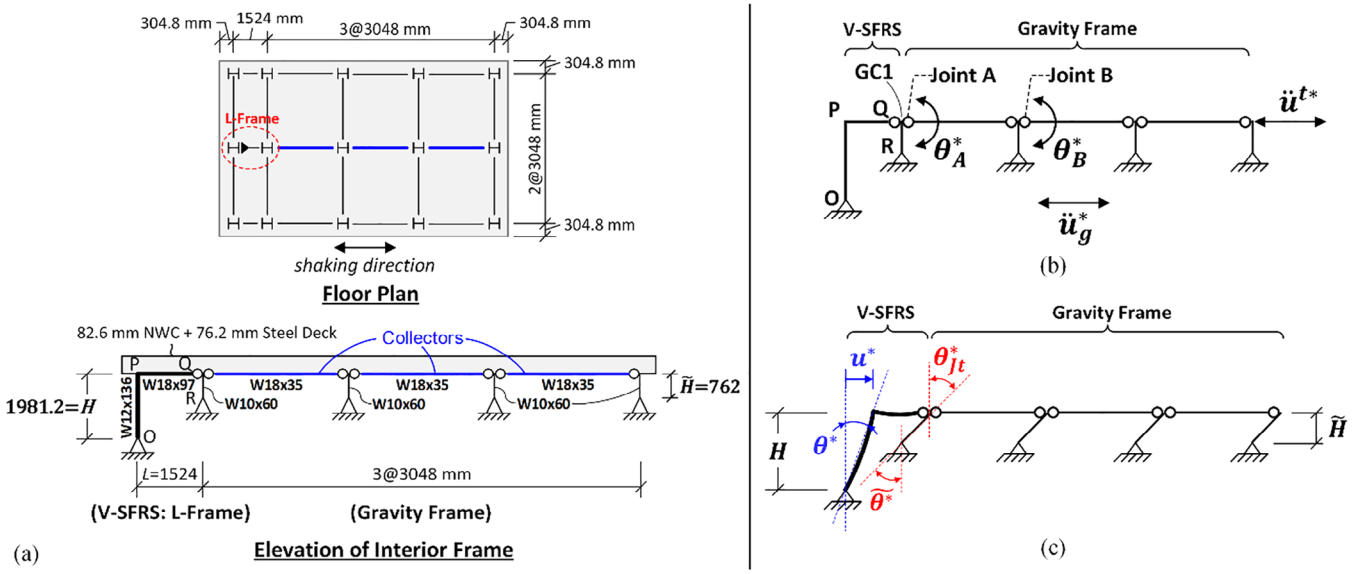

FIGURE 7 | Test building with shortened gravity columns: (a) example structure; (b) analytical model; and (c) associated lateral deformed shape.

joint rotation (θ^*_{Jt}) at the collector ends are the same as gravity frame drift angle, $\widetilde{\theta}^*$. Note that this deformation amplification approach for the gravity frame by shortening the gravity columns can also be applied to the cases where partially-restrained connections are used in the collectors despite possessing a different relationship between the joint rotation (θ^*_{Jt}) and gravity frame story drift ($\widetilde{\theta}^*$).

Furthermore, in order to increase the rotation at joint A, the one-bay MRF (O-P-Q-R) in Figure 3b can be modified to be an L-shaped frame (O-P-Q) in Figure 7a,b and a hinge is inserted at node Q. Since the V-SFRS of the test building is modified, the transfer function and the associated shake table input motion also need to be updated. Figure 8a,b shows the updated collector joint rotation time histories. Although the residual response of the prototype building still cannot be simulated in the test building model and the test building has higher frequency content in the story drift response, the magnitude of the peak joint rotation in the test building is closer to the peak response in the prototype building.

Figure 8c shows a close-up comparison of collector joint rotations between the test and prototype buildings over the 7th to 12th seconds of time history, with Figure 8d showing a comparison of the floor accelerations between the two models within the same time frame. As the test building responds elastically, it is evident that the time histories of its floor absolute acceleration ($\ddot{u}^{t*}$) and collector joint rotation (θ^*_A) are nearly out of phase by 180 degrees, resulting in simultaneous peak floor acceleration and peak deformation (at time t_1). By contrast, in the prototype building, where the structure experiences inelasticity, there is no significant correlation between the floor total acceleration ($\ddot{u}^t_3$) and joint rotation (θ_X). Note that the FAST method is developed to replicate the target floor absolute acceleration, but not intended to produce the correct frequency relationship between story drift and floor acceleration in a multistory prototype structure. While the prototype structure has higher frequency content in the acceleration relative to the drift response, the test specimen's story drift and acceleration are aligned.

In the prototype building, the peak collector joint rotation, concurrent with the peak story drift (at time t_2), does not coincide with the peak floor acceleration (at time t_1). This suggests that the likelihood of simultaneous concurrence of the peak floor accelerations and frame lateral deformation would be low for a building subjected to inelasticity during earthquakes. It is also consistent with the general observation on seismic response of multistory buildings, where each floor reaches its peak acceleration at a different time, which would not necessarily coincide with the peak deformation of the vertical plane SFRS [15, 16]. Furthermore, the analytical results shown in Figure 8 indicate that FAST imposes a more stringent demand—simultaneous peak floor acceleration and adjacent story drift—on the collectors in the test building compared to the commonly observed scenarios—nonconcurrent peak floor acceleration and adjacent story drift—in the inelastic building structures. In other words, FAST is anticipated to create a worst-case scenario for the collectors in the test building once the story drift of the gravity columns in a test building is tuned to match the magnitude of peak response in the prototype structure.

4 | Selection of Test Building Natural Period

For shake table testing with the FAST methodology, this section provides guidelines for the selection and design of a one-story test building. The key parameter is the natural period, which in turn dictates the specimen size (e.g., plan dimensions, members sizes, and story height) and the weight. To address the physical limitations of the maximum acceleration that a given shake table can provide and the desire to produce deformations with a magnitude on the order of practical interest, two useful tools are presented below to bracket the natural period of the test building.

4.1 | Shake Table Input Acceleration Spectrum

The acceleration spectrum of the shake table input motion is used to provide an upper-bound natural period of the test building. For a given target floor acceleration time history, $\ddot{u}^t_{TGT}(t)$ (using

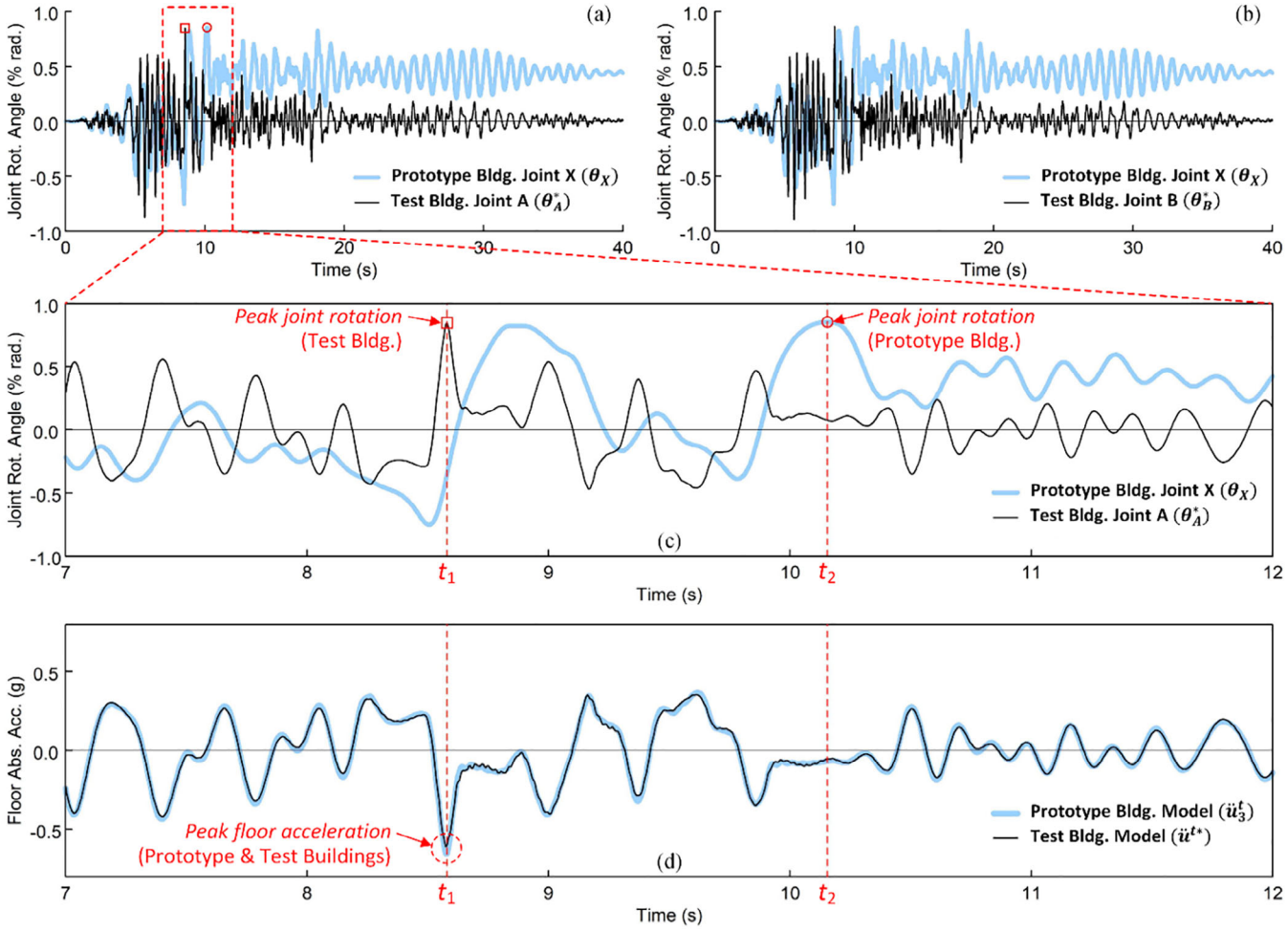

FIGURE 8 | Comparison of analytical history responses between prototype building and test building with shortened gravity columns: (a) θ_X versus θ_A^*; (b) θ_X versus θ_B^*; (c) close-up of θ_X versus θ_A^*; and (d) close-up of $\ddot{u}_3^t$ versus $\ddot{u}^{t*}$.

the 3rd-floor acceleration of the four-story prototype building shown in Figure 4a in this example), a parametric study by varying the natural period (T_n^*) and the damping ratio (ξ^*) of the one-story test building can be conducted for the required input motions. Figure 9 illustrates the procedure to construct an input acceleration spectrum. As shown in Figure 9a, the test building is idealized as an elastic SDOF system and is intended to reproduce $\ddot{u}_{TGT}^t$. The required input acceleration, $\ddot{u}_g^*$, is computed from Equations (7) and (8). Figure 9b shows the computed time histories of required input acceleration, $\ddot{u}_g^*(t)$, for six SDOF systems with $T_n^* = 0.1$, 0.2, or 0.3 s and $\xi^* = 2\%$ or 5% to replicate $\ddot{u}_{TGT}^t(t)$. For each system, the peak absolute value of the input acceleration, $|\ddot{u}_g^*|_{max}$, constitutes one point on the input acceleration spectrum (Figure 9c). Repeating the computations for a range of T_n^* while maintaining ξ^* at a specific value produces the spectrum curve for that specific ξ^* value.

Figure 9c demonstrates the input acceleration spectrum curves for $\xi^* = 0\%$, 2%, 5%, and 10% for replicating the target response $\ddot{u}_{TGT}^t(t)$ (Figure 9a-right). It is evident that all the spectrum curves rise dramatically with an increase of T_n^* except for a slight decay of spectral acceleration in the short period range (approximately $T_n^* \leq 0.120$ s). In general, the longer the natural period of the test building, the higher the required magnitude of input acceleration. In addition, the comparison among the spectrum curves with different ξ^* shows that an increase in damping ratio would help lower the spectral acceleration (i.e., the required peak input acceleration). At the left end ($T_n^* = 0$) of each spectrum curve, where the test building is infinitely stiff, the spectral acceleration equals to the peak absolute value of the target floor acceleration, $|\ddot{u}_{TGT}^t|_{max}$, as a result of that the rigid structure does not deform during the shaking so that its floor total acceleration is identical to the input acceleration. The spectral accelerations decline with T_n^* in the short period range because the structure is stiff enough to sustain its relative acceleration ($\ddot{u}^*$) to act almost in the same phase as the input acceleration ($\ddot{u}_g^*$). As $\ddot{u}^*$ and $\ddot{u}_g^*$ act in the same phase while the relation $\ddot{u}^{t*} = \ddot{u}_{TGT}^t = \ddot{u}^* + \ddot{u}_g^*$ holds, the relation $|\ddot{u}_{TGT}^t| = |\ddot{u}^*| + |\ddot{u}_g^*|$ can be established. In this case, an increase in the natural period T_n^*, which tends to increase the magnitude of structural response (i.e., $|\ddot{u}^*|$), would cause a decrease in the amplitude of required input motion (i.e., $|\ddot{u}_g^*|$) to reach the same target response $\ddot{u}_{TGT}^t$. By contrast, for the remaining range of natural periods, the structure response ($\ddot{u}^*$) and input motion ($\ddot{u}_g^*$) are not in the same phase and tend to be out of phase, leading to the relation $|\ddot{u}_{TGT}^t| = |\ddot{u}^*| - |\ddot{u}_g^*|$. In this case, an increase in T_n^*, which tends to increase $|\ddot{u}^*|$, would cause a rise in $|\ddot{u}_g^*|$ to reach a given target $\ddot{u}_{TGT}^t$.

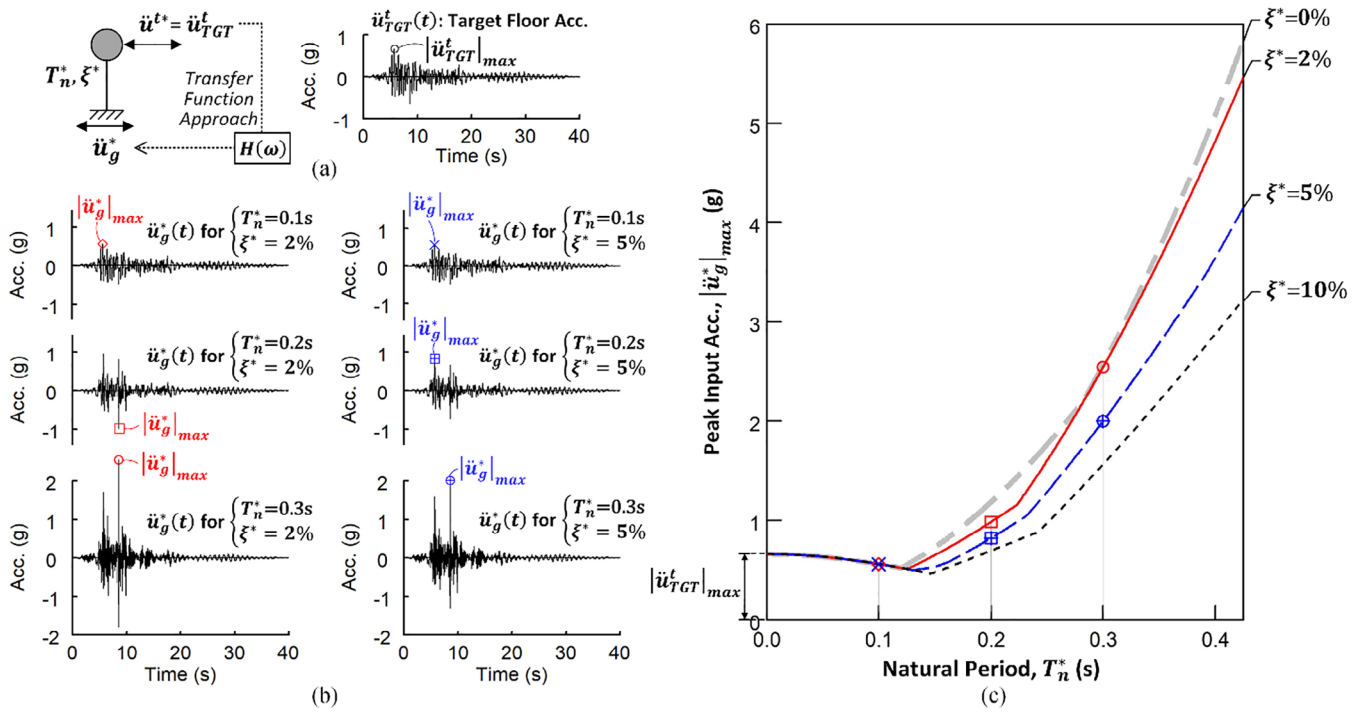

FIGURE 9 | (a) Target total acceleration ($\ddot{u}^t_{TGT}$) time history for an SDOF system representing a FAST specimen; (b) required input accelerations ($\ddot{u}^*_g$) for SDOF systems with $T^*_n = 0.1$, 0.2, or 0.3 s and $\xi^* = 2\%$ or 5%; and (c) input acceleration spectrum.

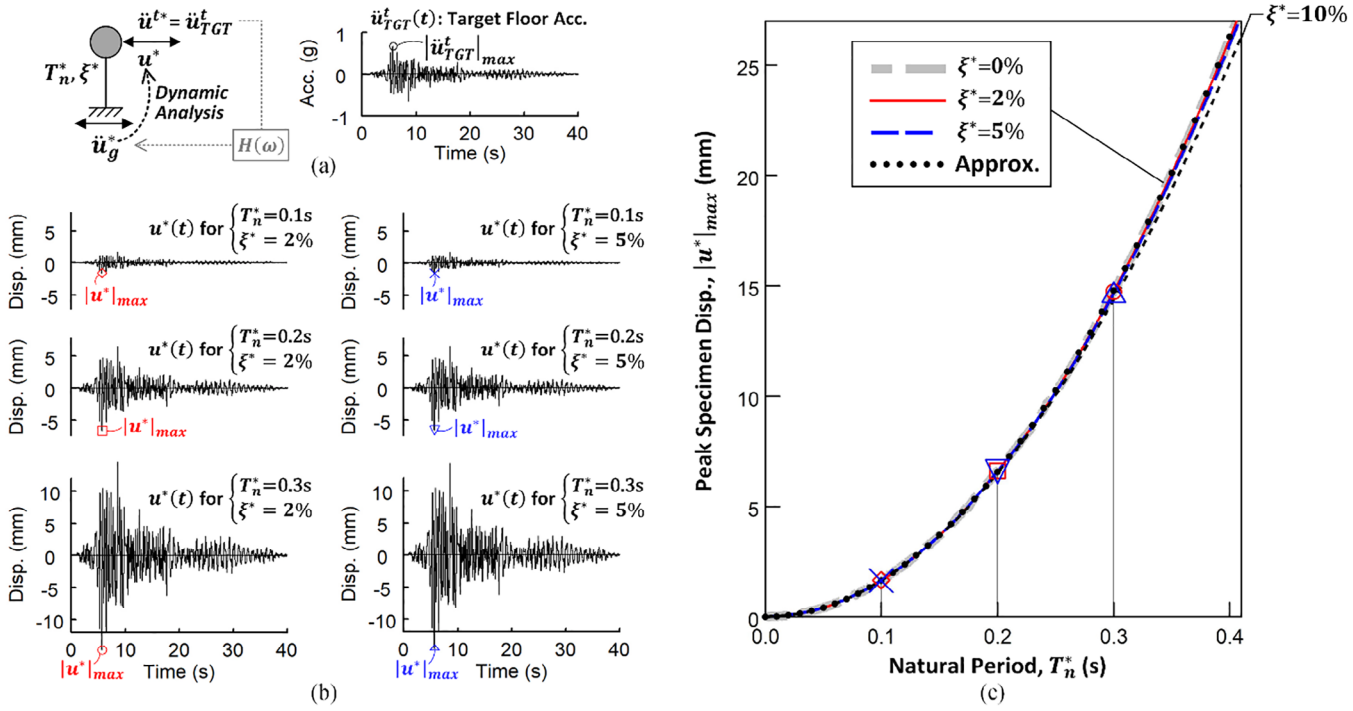

FIGURE 10 | (a) Target total acceleration ($\ddot{u}^t_{TGT}$) time history for an SDOF system representing a FAST specimen; (b) displacement (u^*) time histories for SDOF systems with $T^*_n = 0.1$, 0.2, or 0.3 s and $\xi^* = 2\%$ or 5%; and (c) specimen displacement response spectrum.

4.2 | Specimen Displacement Spectrum

The displacement spectrum of the specimen is used to identify the lower-bound natural period of a test building. Figure 10 shows the procedure to construct a specimen displacement spectrum for the FAST method. As illustrated in Figure 10a, while an elastic SDOF system is producing the target total acceleration $\ddot{u}^t_{TGT}(t)$ (using the 3rd-floor response of the prototype building shown in Figure 4a as an example again), its relative displacement time history, $u^*(t)$, can be determined by conducting a dynamic

analysis (e.g., Duhamel's integral or Newmark's method) on the same SDOF system with the input motion $\ddot{u}_g^*(t)$. Figure 10b shows $u^*(t)$ of six SDOF systems with $T_n^* = 0.1$, 0.2, or 0.3 s and $\xi^* = 2\%$ or 5%, respectively, with all the SDOF systems reproducing $\ddot{u}_{TGT}^t(t)$. For each system, the peak value of the displacement history response, $|u^*|_{max}$, constitutes one point on the displacement response spectrum (Figure 10c). By repeating these computations across a range of T_n^* values for a given ξ^*, the displacement spectrum curve for that ξ^* value can be generated.

Figure 10c demonstrates the specimen displacement spectra for $\xi^* = 0\%$, 2%, 5%, and 10%. It shows that the peak displacement is insensitive to the damping for lightly damping structures (say, up to a damping ratio of 10%). The spectrum curve, which can be approximated by a quadratic function, indicates that the displacement would increase rapidly with an increase of the natural period, T_n^*. The quadratic nature of the spectrum shape can be demonstrated from the equation of motion:

$$m\ddot{u}^{t*}(t) + c\dot{u}^*(t) + ku^*(t) = 0 \tag{9}$$

The second term, $c\dot{u}^*$ (i.e., damping force), can be ignored at the instant when the peak displacement is reached. As the FAST specimen is intended to reproduce target floor acceleration, $\ddot{u}^{t*}(t) = \ddot{u}_{TGT}^t(t)$ can be substituted into Equation (9). The equation of motion at the peak displacement can be simplified as:

$$m\ddot{u}_{TGT}^t + ku^* = 0 \tag{10a}$$

that is,

$$u^* = -\left(\frac{m}{k}\right)\ddot{u}_{TGT}^t \tag{10b}$$

Then, the absolute value of peak displacement can be approximated as follows:

$$|u^*|_{max} = \left(\frac{m}{k}\right)|\ddot{u}_{TGT}^t|_{max} = \left(\frac{T_n^*}{2\pi}\right)^2 |\ddot{u}_{TGT}^t|_{max}$$

$$= \left[\frac{|\ddot{u}_{TGT}^t|_{max}}{4\pi^2}\right](T_n^*)^2 \tag{11}$$

As shown in Figure 10c, the approximation quadratic curve (labeled as "Approx.") derived from Equation (11) aligns well with the displacement response spectrum curves of lightly damped systems.

4.3 | Determination of Applicable Period Range

Lastly, Figure 11 demonstrates how to use the two types of spectra to bracket the natural period for the test specimen used in the FAST. Figure 11a shows the use of a shake table input acceleration spectrum to identify the upper-bound natural period, $T_{n,UB}^*$, of the test building. Assuming the shake table's acceleration is limited to 4 g, $T_{n,UB}^*$ equals 0.366 s for a test building with an estimated damping ratio of 2%. Figure 11b shows schematically the deformation response spectra for two different gravity column heights. From the perspective of specimen design, the story drift angle of the gravity frame, $\tilde{\theta}^*$, is a quantity more meaningful than

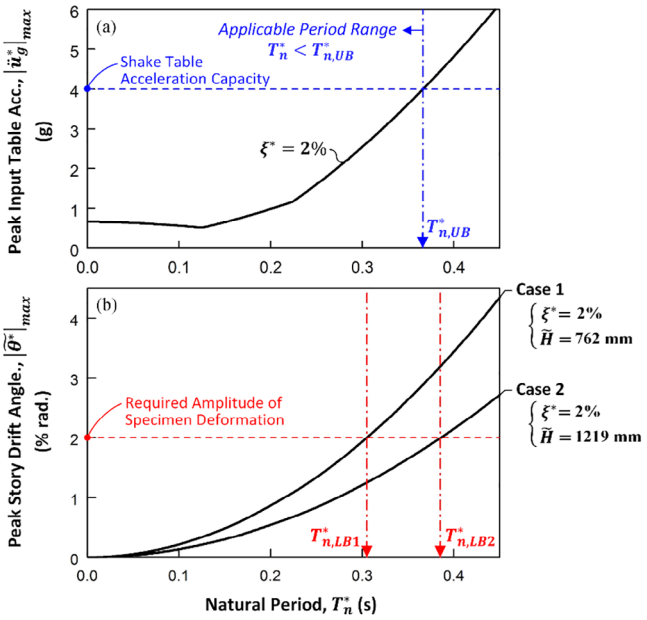

FIGURE 11 | Determination of applicable period range for a specimen by using (a) input acceleration spectrum in conjunction with (b) specimen deformation spectrum.

the relative displacement of the one-story test building. It was shown in Figure 8 that adjusting the length of gravity columns can be used to achieve the desirable level of gravity frame story drift ($\tilde{\theta}^*$) and the collector end rotations in the test building. The deformation spectrum for $\tilde{\theta}^*$ (Figure 11b) can be obtained by dividing the relative displacement spectrum (Figure 10c) by the gravity column length, $\tilde{H}$. Taking 0.02 radian as the required magnitude of story drift, a lower-bound period ($T_{n,LB1}^*$ or $T_{n,LB2}^*$) can be determined for each case. Together with the upper-bound period $T_{n,UB}^*$ obtained in Figure 11a,b shows that Case 2 with $\tilde{H} =$ 1219 mm is not feasible as $T_{n,LB2}^* > T_{n,UB}^*$. Instead, Case 1 with $\tilde{H} =$ 762 mm has a feasible range of natural period between $T_{n,LB1}^*$ and $T_{n,UB}^*$.

5 | Experimental Verification

5.1 | General Test Program

Experimental validation of the proposed FAST methodology constituted Phase 1 of a shake table test program on a half-scale, one-story steel building. The testing was conducted at the NHERI@UCSD LHPOST facility to explore the seismic response of collectors in steel structures [17] as part of a larger multi-university project studying steel seismic collectors [5]. For this research, a 12-story steel BRBF archetype building designed by Torabian et al. [18] was chosen as the prototype structure (see Figure 1a). A 2-D frame model was developed in PISA3D to represent half of the prototype building. The modeling procedure is similar to that described earlier for the numerical simulation of a 4-story BRBF building. The analytical periods of the first three modes (T_1, T_2, and T_3) are 2.833, 1.005, and 0.594 s, respectively. NLRHAs were conducted on this model to obtain its floor acceleration response under input ground motions. Finally, three FASTs were executed to excite the single-story

test building, reproducing three target floor acceleration time histories. These histories were determined based on the 5th-floor acceleration responses of the PISA3D prototype model subjected to historical ground motions scaled to 20%, 50%, and 100% of design earthquake levels [14]. The reason for selecting the 5th-floor acceleration is because it has high frequency contents in the 2nd and 3rd modes, representing a higher-mode dominated response as commonly seen in floor acceleration responses in the multistory building.

5.2 | Specimen Design

A half-scale, single-story steel building with a composite floor slab (Figure 12a) was designed and then constructed on the shake table. As illustrated in Figure 12b, the building's floor plan measured 11.582 m in length and 5.486 m in width. The composite floor, comprising a 51-mm concrete slab atop a 38-mm metal deck, extended 305 mm beyond the beam centerlines along the building's perimeter. In the longitudinal (West–East) direction, which coincided with the direction of shaking, the building featured two bays each spanning 4267 mm, along with one 1524-mm bay and a 1524-mm cantilever span. The specimen incorporated two longitudinal perimeter frames positioned at the north and south faces. Within each longitudinal frame (Figure 12c), a W12 × 170 steel column, functioning as a cantilever column, was situated at the west end (on Column Line 1) to serve as the V-SFRS. The beamline extending to the east from each cantilever column was designed to serve as the seismic collector. Aside from the two cantilever columns and the collectors, the remaining components of the specimen constituted the gravity frame. Each cantilever steel column was embedded into a 914-mm tall reinforced concrete footing (identified as RC footing 1), which was affixed to the shake table via tie-down rods to mimic a fixed-base condition for the steel column. Furthermore, the three remaining W8 × 40 columns (on Column Lines 1, 2, and 3) in each longitudinal frame were pin-supported and acted as gravity columns. A pin-support, constructed using a steel fixture with a 25 mm-diameter A325 bolt as the "pin", was positioned beneath each gravity column and connected to the base plate of the column via bolts. Beneath each pin-support, a 1422-mm tall RC footing (designated as RC footing 2 or 3) was installed to serve as a spacer. Both the pin-support and the RC footing spacer were secured to the shake table.

To withstand longitudinal shaking, as depicted in Figure 12a, perimeter beams within the south and north frames functioned as collectors, while those situated at the west and east sides of the floor diaphragm acted as chords. Each collector beam line was assigned four collectors from west to east, denoted as Collectors 1, 2, 3, and 4, respectively. Collectors 1 and 2, spanning 4267 mm, were constructed using W14 × 30 beams, whereas Collectors 3 and 4, measuring 1524 mm, along with the two chords and the remaining floor beams, utilized W14 × 26 beams. Figure 12c illustrates three types of collector-to-column connections: all-flange weld (AFW), top flange weld (TFW), and bolted-web (BW) details. All beam-to-girder and beam-to-column connections for the other floor beams employed the BW detail.

In each longitudinal frame, a diagonal brace was utilized to support the cantilever span illustrated in Figure 12c. As depicted in Figure 12a, for the transverse direction of the specimen, four single-bay chevron braced frames were deployed on Column Lines 1, 2, 3, and 4 to counteract torsional forces and translational motion perpendicular to the shaking direction. All W-shape members were fabricated from A992 steel, while braces were constructed using long leg back-to-back A36 double angle sections of 2L5 × 3 × 3/8 dimensions. All plates, including continuity plates, stiffeners, and gusset plates, were specified to be A572 Gr. 50 steel. The composite slab consisted of 20-gauge Verco PLB-36 deck and lightweight concrete with a specified strength of f'_c = 27.5 MPa. Additional mass was incorporated using RC blocks, attached to the composite slab via posttensioning (PT) rods. As shown in Figure 12, four groups of these added mass blocks were distributed over the four spans of the building in the longitudinal direction. The four groups of added weights, arranged from west to east, were 11,802, 12,247, 5194, and 7312 kgf, respectively.

It is worth noting that the cantilever column, which occupies the least floor area among the types of V-SFRS, was chosen for the test building. This selection aimed to maximize the length and tributary area for the main subject of the study, namely the steel seismic collectors residing in the floor system. For the specimen design, the V-SFRS (i.e., the cantilever columns) were sized to possess sufficient stiffness such that the fundamental period (T_n^*) of the test building is within the applicable range which has upper bound period, $T^*_{n,UB}$, corresponding to a shake table acceleration limitation of 3.44 g with respect to a target floor acceleration at an 2.0 times DE intensity level. Note that, although the specimen was designed for an intensity up to 200% of DE level, the highest intensity level reached in this Phase 1 testing was only 100% of DE because the entire test program contained multiple phases, and it was intended to skip the high-intensity tests to avoid the damage of the specimen in Phase 1. By employing varying heights of RC footings between the cantilever columns and gravity columns, the story heights of the gravity column ($\tilde{H}$= 1930 mm) were intentionally made shorter than those of the V-SFRS (H = 2438 mm) in order to amplify the story drift and collector joint rotations, thereby facilitating the research objectives with respect to the seismic collectors. It is noted that, even though the analytical study presented earlier (Figures 7 and 8) has shown that it is possible for the test specimen to achieve the desirable story drift similar to that expected in the prototype structure, this study did not specifically adjust the specimen story drift to match the magnitude of the prototype structure response for two reasons. The first reason is related to the height of the test specimen. Given the "reasonable" size and height of the cantilever column for this test program, the required height of the gravity columns would be much shorter than that actually used, which was judged not practical. The second reason is associated with the shear capacity of the composite floor diaphragm. The desirable reactive weight from the added concrete blocks that could be placed on the floor, which was limited by the area of the shake table, was reduced to avoid shear failure of the diaphragm.

5.3 | Test Procedure and Generation of Input Motion

Three shake table tests (FAST-1, FAST-2, and FAST-3) were conducted. The purpose of these FAST tests was to reproduce

(a)

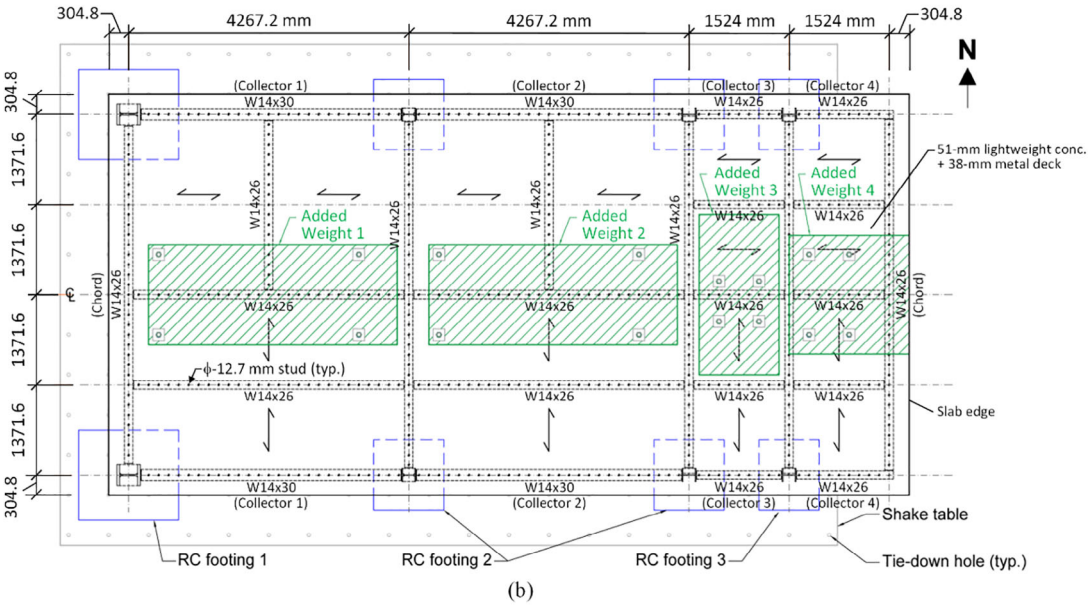

(b)

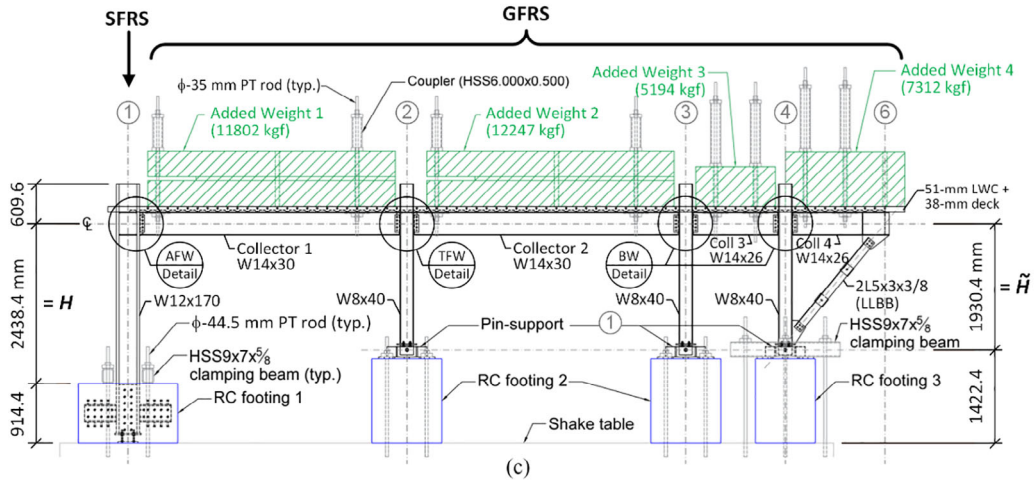

(c)

FIGURE 12 | Test building: (a) overview photo; (b) floor plan; and (c) elevation of longitudinal frame.

floor acceleration responses corresponding to 20%, 50%, and 100% of the design earthquake (DE), respectively. Dynamic characterization tests, which included white noise (WN) tests as well as impulse (IM) tests, were conducted to evaluate the dynamic properties of the specimen both before and after each FAST test (see Table 1). The natural period and damping characteristics assessed from the dynamic characterization tests preceding each FAST test were utilized to generate the transfer function for computing the input motion for that specific FAST test.

Figure 13 depicts the detailed procedure employed in this test program for conducting each FAST. This procedure is summarized into five steps as described below:

TABLE 1 | Test matrix.

Test ID	Testing method	Intensity
WN-0	White noise test	PGA = 0.1 g
IM-0	Impulse test	PGA = 0.2 g
FAST-1	Floor acceleration simulation test	20% design earthquake (PGA = 0.37 g)
IM-1	Impulse test	PGA = 0.2 g
FAST-2	Floor acceleration simulation test	50% design earthquake (PGA = 0.95 g)
IM-2	Impulse test	PGA = 0.2 g
FAST-3	Floor acceleration simulation test	100% design earthquake (PGA = 1.65 g)
WN-3	White noise test	PGA = 0.1 g
IM-3	Impulse test	PGA = 0.2 g

- Step 1: An NLRHA was conducted to obtain the floor absolute acceleration time history of the prototype structure, denoted as $\ddot{u}^t(t)$. For this analysis, a ground motion record (Beverly Hills-14145 Mulhol Station) from the 1994 Northridge Earthquake was scaled so that its spectral acceleration matches 20%, 50%, or 100% of a DE spectrum. The DE spectrum was constructed based on $S_{DS} = 1.03$ and $S_{D1} = 0.569$ [14] at the first mode period of the prototype building model. The numerically calculated 5th-floor acceleration history response, $\ddot{u}^t_5$, with a duration $t_d = 30$ s, was chosen as the target response for the test specimen.
- Step 2: Since the test specimen was a 50%-scale model (i.e., scale factor $l_d = 0.5$), the time scale of $\ddot{u}^t(t)$ was initially adjusted by a factor of $\sqrt{l_d}$. The adjusted $\ddot{u}^t_{TGT}(t)$ underwent modification via signal processing techniques such as resampling, filtering, and detrending. The detrending process employed here not only eliminated a polynomial trend from the displacement data obtained by double integrating the acceleration record but also incorporated a polynomial taper (with a duration t_{taper} about 1 s) at each end of the displacement data. This measure ensured that the processed acceleration, velocity, and displacement all approached zero at both ends of the time history. Consequently, the finalized $\ddot{u}^t_{TGT}(t)$ possesses a duration of $t^*_{do} = \sqrt{l_d} t_d + 2t_{taper}$.
- Step 3: Dynamic characterization tests were conducted to experimentally determine dynamic properties T^*_n and ξ^* such that the transfer function $H(\omega)$ according to Equation (7) could be established. The required input table motion $\ddot{u}^*_{go}(t)$ was then determined by performing an inverse FFT of its frequency-domain counterpart $\ddot{u}^*_{go}(\omega)$, which was computed from Equation (8). The subscript "o" in $\ddot{u}^*_{go}$ means that the signal is prior to the final signal processing.
- Step 4: Filtering, detrending, and zero padding were applied to $\ddot{u}^*_{go}(t)$ to obtain the finalized input motion $\ddot{u}^*_g(t)$.
- Step 5: FAST was performed with $\ddot{u}^*_g(t)$ as the table input motion

5.4 | Test Results

Table 2 presents a summary of the results obtained from the dynamic characterization tests. Throughout the entire testing, the fundamental period of the specimen, denoted as T^*_n, remained relatively constant with only a slight decay observed. In addition, the measured damping ratio, denoted as ξ^*, ranged from 3.03% to 3.50%. The measured sensor signals were filtered using an 8th-order Butterworth low-pass filter with a cutoff frequency of 30 Hz. Figure 14 shows the global responses of the specimen for the three FAST tests conducted. Peak floor accelerations achieved during FAST-1, FAST-2, and FAST-3 were 0.41, 0.93, and 1.53 g, respectively. The peak story drift angles reached were 0.11% rad, 0.32% rad, and 0.62% rad for the three tests, respectively, which were lower than the analytical peak interstory drifts of 0.38% rad, 0.87% rad, and 1.87% rad, respectively, obtained from the 4th story, which is adjacent to and below the target 5th floor, of prototype structure model for three intensity levels (20%, 50%, and 100% of DE) of NLRHAs. Although the test building was configured with shorter gravity columns to amplify the story drift angle response of the gravity frame relative to the LFRS, the columns were not sufficiently short to match the magnitude of the prototype's response, due to practical limitations and the desire to avoid secondary (e.g., catenary) effects. As a result, the test specimen's peak story drift angle, while closer to the intended target due to this measure, still remained considerably smaller than those of the analytical prototype model.

Furthermore, as shown in Figure 14a–c, the base shear versus story drift relationships observed in all three tests were basically linear, indicating that the specimen remained within the elastic range throughout the testing program. Due to space constraints, the subsequent sections will delve into the detailed results of the FAST-3 test, which experienced the highest intensity. In the following, the assessment is focused on the effectiveness and issues of implementing FAST to simulate the floor acceleration responses from two perspectives: the response amplitude and frequency content.

To illustrate the detailed FAST-3 test results, Figure 15 depicts a comparison between the measured and command signals for the input table acceleration, $\ddot{u}^*_g$, while Figure 16 shows the comparison between the measured and target floor accelerations, $\ddot{u}^{t*}$ and $\ddot{u}^t_{TGT}$. Within the plots of pseudo-spectra acceleration (PS_a) showcased in Figures 15d and 16d, the natural periods of the first three translational vibration modes in the direction of shaking (T^*_1, T^*_2, and T^*_3) for a 0.5-scale model representing the prototype

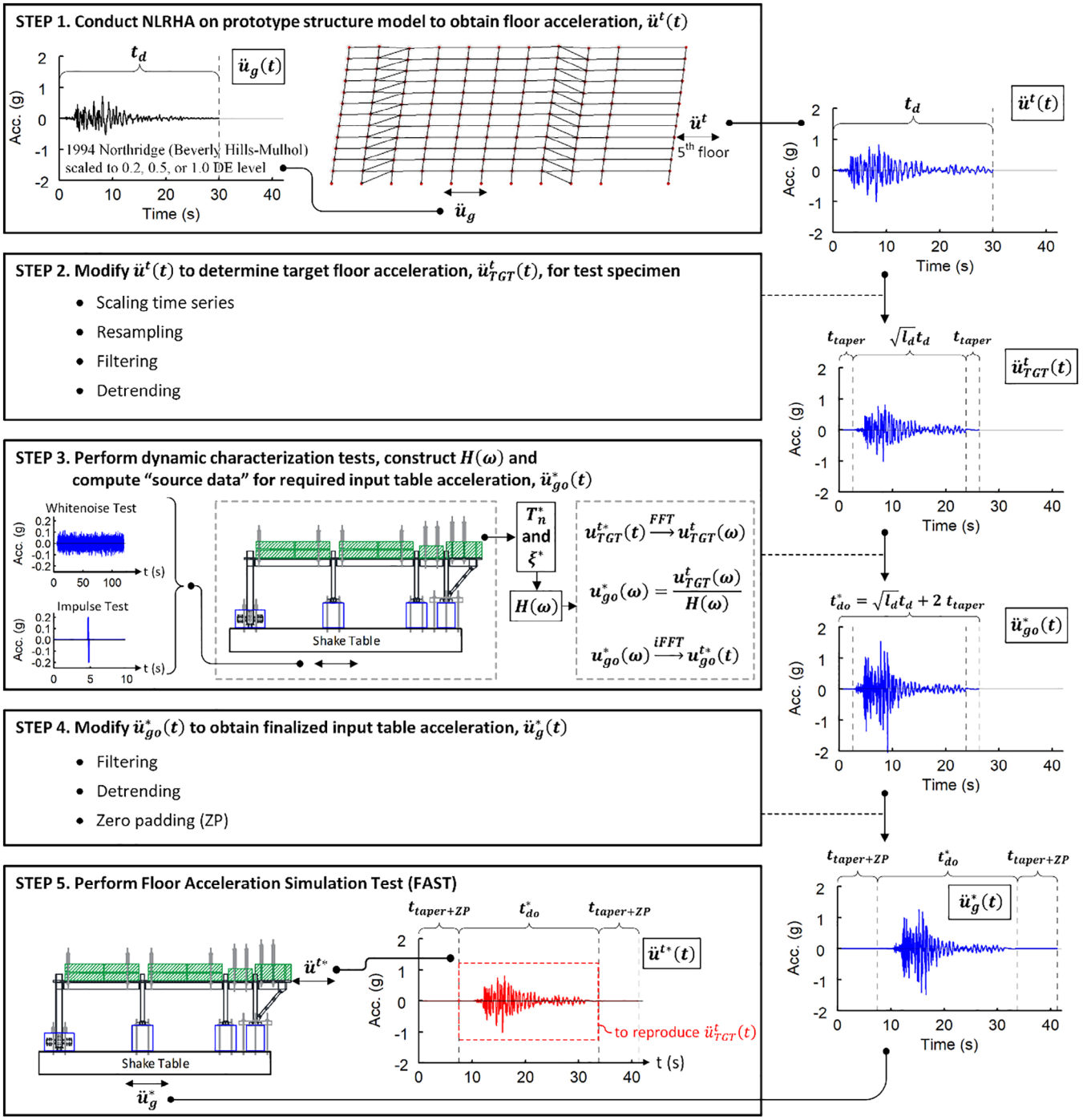

FIGURE 13 | Schematics of test procedure and generation of input acceleration.

TABLE 2 | Dynamic characterization test results.

Test timing	Impulse test			White noise test	
	Test ID	T_1^* (sec)	ξ^* (%)	Test ID	T_1^* (sec)
Before FAST-1	IM-0	0.174	3.19	WN-0	0.172
After FAST-1	IM-1	0.175	3.03	–	–
After FAST-2	IM-2	0.177	3.10	–	–
After FAST-3	IM-3	0.182	3.50	WN-3	0.179

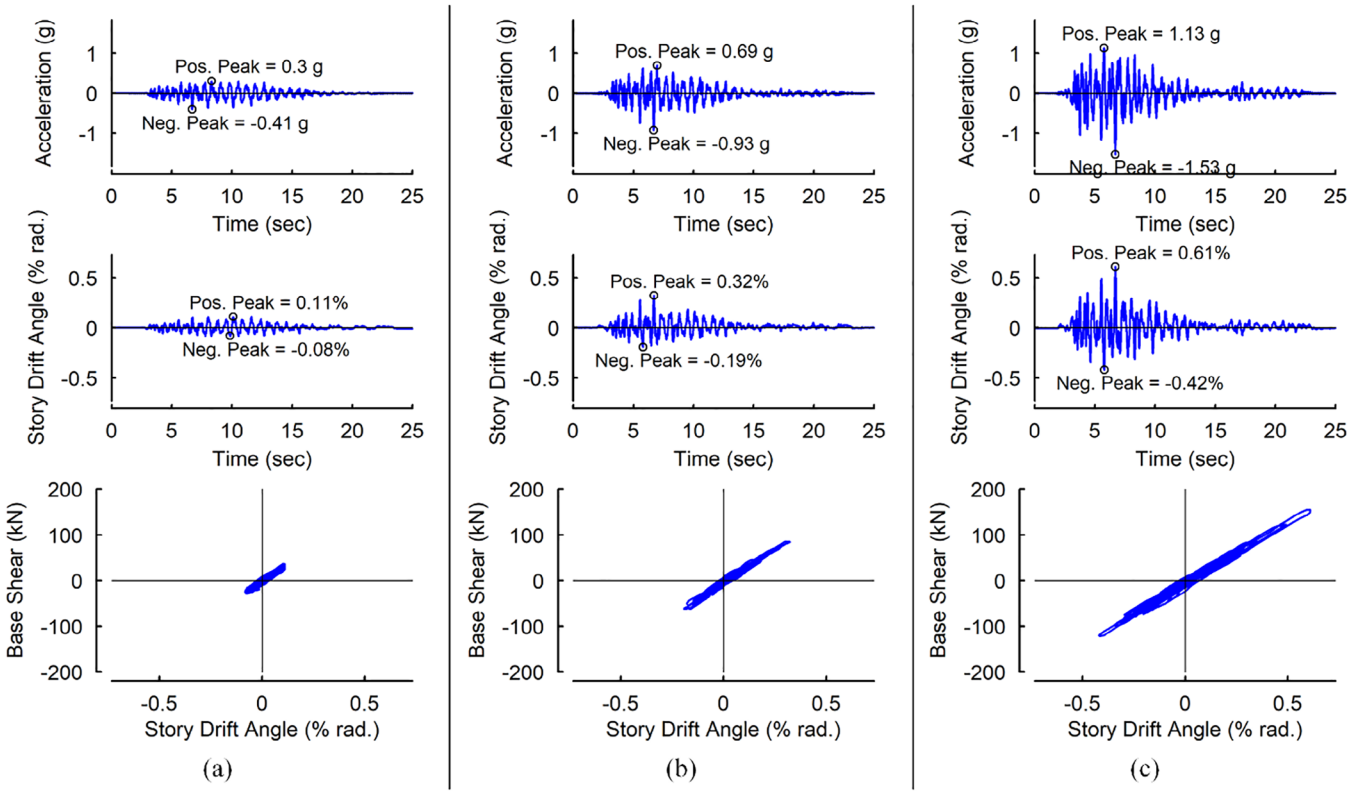

FIGURE 14 | Floor acceleration (top row), story drift angle (middle row), and base shear versus story drift angle relationship (bottom row) of specimen in (a) FAST-1, (b) FAST-2, and (c) FAST-3.

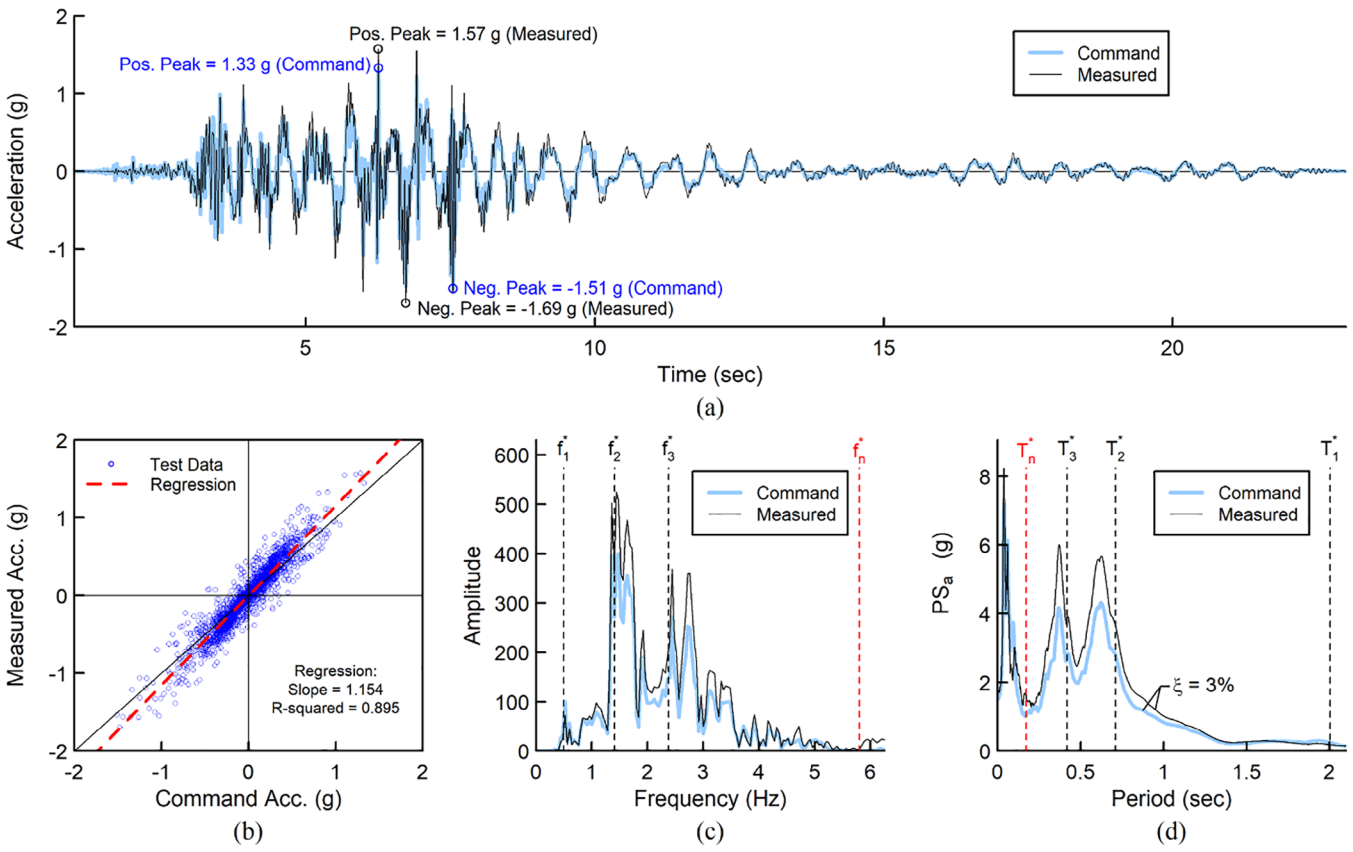

FIGURE 15 | Comparison of measured and command signals for input acceleration, $\ddot{u}_g^*$, for FAST-3: (a) time histories; (b) measured versus target responses relation; (c) fast Fourier transforms; (d) response spectra.

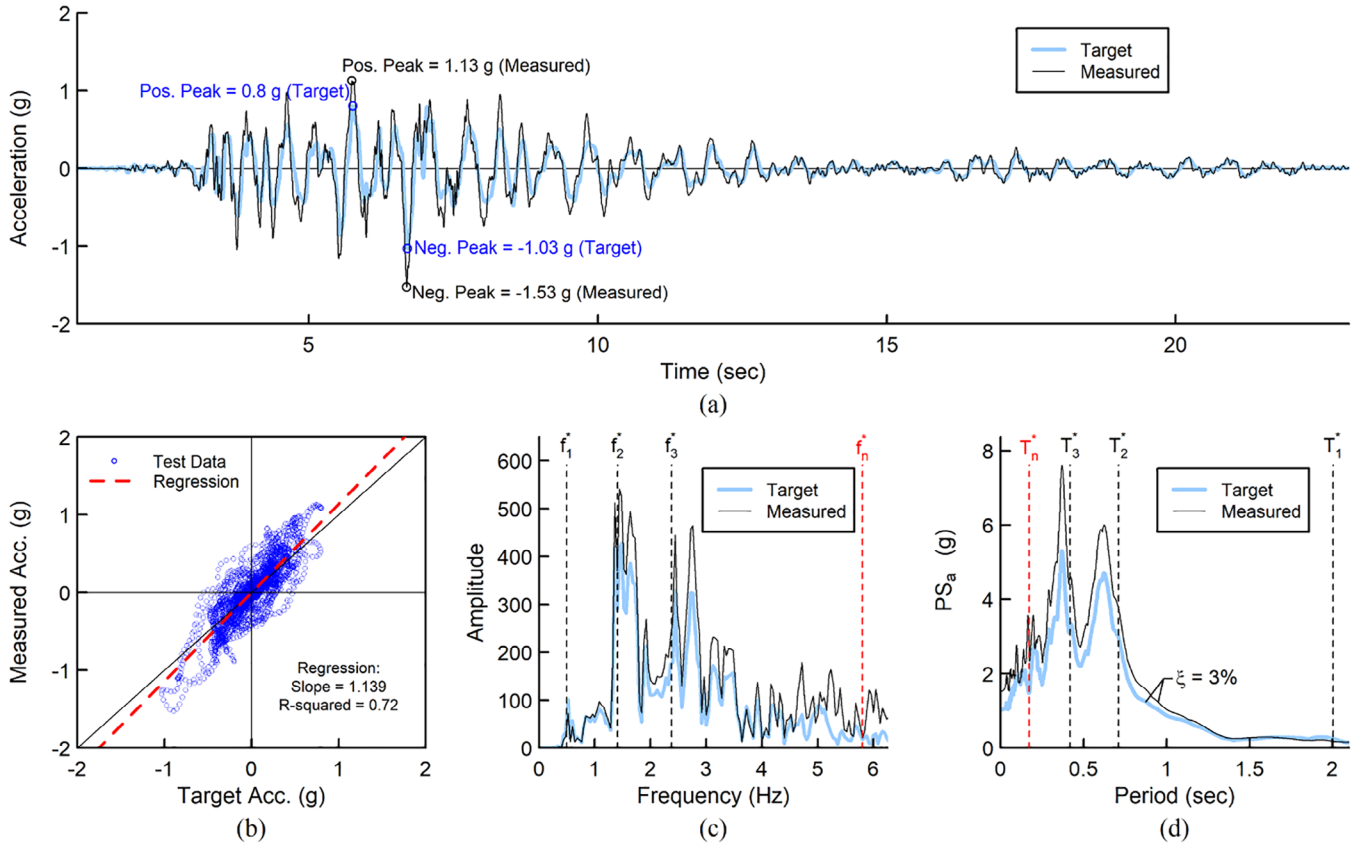

FIGURE 16 | Comparison of measured and target output accelerations, $\ddot{u}^{t*}$ and $\ddot{u}^{t}_{TGT}$, for FAST-3: (a) time histories; (b) measured versus target responses relation; (c) fast Fourier transforms; (d) response spectra.

structure are delineated. Note that these periods are determined by scaling the analytical periods of the first three modes of the prototype structure model (T_1, T_2, and T_3), respectively, by a factor of $\sqrt{0.5}$. Furthermore, the specimen's natural period, T_n^*, is also indicated in the figure. Similarly, in the fast Fourier transform (FFT) graphs presented in Figures 15c and 16c, the natural frequencies f_1^*, f_2^*, f_3^*, and f_n^*, which correspond to T_1^*, T_2^*, T_3^*, and T_n^*, respectively, are highlighted.

The fidelity of the shake table used in this test program is evaluated first. Figure 15a illustrates that the time history of the measured shake table input acceleration did not precisely match the commanded input motion. The measured peak accelerations reached +1.57 g and −1.69 g, surpassing the peak values (+1.33 g and −1.51 g, respectively) of the target input motion. As depicted in Figure 15b, the scatter plot comparing actual versus target input motions reveals a strong linear relationship, with a slope of 1.154 and an R-squared value of 0.895. This indicates an overshoot of approximately 15% in achieving the table acceleration compared to the target input motion. Analysis of both the FFT and PS_a spectra, depicted in Figure 15c,d respectively, shows similar spectral shapes for the two signals, albeit with the amplitude of the measured table acceleration generally higher than that of the commanded input motion.

Figure 16a shows a comparison of the time histories of the measured and target floor accelerations, which are denoted as $\ddot{u}^{t*}$ and $\ddot{u}^{t}_{TGT}$, respectively. The measured peak accelerations reached +1.13 g and −1.53 g, exceeding the peak values of the target floor acceleration (+0.80 g and −1.03 g, respectively). Nevertheless, Figure 16b shows a positive correlation between $\ddot{u}^{t*}$ and $\ddot{u}^{t}_{TGT}$. A linear regression analysis yielded a slope of 1.139 with an R-squared value of 0.720, indicating that an overshoot (14%) of the floor acceleration is mainly due to the 15% overshoot of the table input motion (see Figure 15b) and other factors associated with the unavoidable interaction between the specimen and the shake table hydraulic system.

The FFT plots (Figure 16c) and PS_a spectra (Figure 16d) for both signals ($\ddot{u}^{t*}$ versus $\ddot{u}^{t}_{TGT}$) reveal similar spectral shapes, suggesting that the achieved floor acceleration captures the dynamic characteristics of the target response. However, the amplitudes of peaks in the FFT or PS_a spectrum of $\ddot{u}^{t*}$ are higher than those of $\ddot{u}^{t}_{TGT}$, consistent with the observed overshooting in Figure 16b. Additionally, Figure 16c,d indicates that both target and measured floor accelerations have high frequency contents at the 2nd and 3rd modes of a scaled model representing the prototype structure. This higer-mode dominated response pattern is typical in the floor accelerations of multistory buildings. It is worth noting that although the test specimen has a natural frequency (f_n^*) or period (T_n^*) different from those of the 2nd and 3rd modes of the scaled model for the prototype building, the proposed test methodology successfully made the specimen floor acceleration exhibit a spectral shape resembling that of the target response.

It is important to note that while an overall 14% overshooting of the test specimen's floor acceleration seems moderate

(Figure 16b), the specimen's peak acceleration (−1.53 g) exceeded the target response (−1.03 g) by about 50% (Figure 16a), which is significant. This "amplification" of the floor acceleration near the peak response may be attributed to the interaction between the shake table and specimen. This suggests that, to enhance the accuracy of the FAST in reproducing the target specimen response, measures addressing structure-table interaction and reducing shake table tracking errors of the input motion command must be implemented. In practice, an iterative process [19, 20] of tuning of the shake table can be conducted before tests to enhance the accuracy in reproduction of prescribed table motion.

6 | Summary and Conclusions

In this research, the FAST methodology, which employs a transfer function approach to compute the required input motion for shake table testing, is proposed to excite an elastic one-story test building to replicate a specified target absolute acceleration response originating from a chosen floor of a multistory prototype building experiencing nonlinear behavior during a seismic event. As the FAST enables the simulation of real inertial force mechanisms including higher-mode effect in a single-story test specimen and the use of elastic test specimen also allows for the reusability of the specimen, this method enhances the efficiency of shake table testing and is particularly suitable for research on floor diaphragm systems or nonstructural components, where the governing force demands correspond to the seismic floor accelerations.

The one-story test specimen for the FAST methodology is suggested to be composed of an SFRS, gravity columns, and a floor diaphragm and to be designed such that the SFRS serves as a vehicle to replicate the target floor acceleration, while the floor diaphragm and/or its components are the main subject of the investigation. Analytical studies validate that adjusting the length of gravity columns can be used to achieve the desirable level of story drift of the gravity frame and the collector end rotations in the test building. This paper also presents the guidelines of developing response spectra for the input table acceleration and the specimen displacement for using the FAST methodology to replicate a specific target floor acceleration. By considering the shake table capacity and the desired specimen deformation as constraints, these response spectra can be employed collectively to determine the viable range of natural periods for the test specimen.

Experimental validation of the FAST methodology was carried out on a half-scale, single-story steel building featuring a composite floor slab, utilizing the NHERI@UCSD LHPOST facility. Despite the measured floor acceleration in the test specimen exceeding the target response due to the input table motion overshoot resulting from the interaction between the specimen and shake table, test results confirmed that the FAST accurately reproduced the intended frequency content—which reflects the higher-mode effects of the multistory prototype building—in the "SDOF-like" single-story test building. Although the proposed methodology cannot reproduce the story drift response, using shorter gravity columns is proposed to mitigate this shortcoming and has been verified analytically. In this research, this remedy was not fully applied due to some limitations in the specimen design. Hence, the story drift responses in the test building were smaller than those of the analytical prototype structure.

Acknowledgments

This research was supported by the National Science Foundation (NSF), Engineering for Natural Hazards (ENH) program under Grant CMMI-1662816 and Supplement CMMI-1937703. Any opinions, findings, conclusions or recommendations expressed in this material are those of the author(s) and do not necessarily reflect the views of the NSF. The authors also would like to acknowledge the following industrial partners for their donations to the test program: American Institute of Steel Construction (AISC), The California Field Ironworkers Administrative Trust, The Herrick Corporation, Annie-Johnson Company, CoreBrace LLC, Testing & Inspection Service. Messrs. J. Malley (Degenkolb Engineers), R. Sabelli (Walter P. Moore), R. Lobo, A. Sumer, and C. Tokas (HCAI), L. Kruth and T. Schlafly (AISC) served on the Industrial Advisory Panel. The authors are grateful for this support. In addition, the authors would like to thank Messrs. A. Sherman, R. Beckley, and J. Fitcher, staff members of NHERI@UCSD large high performance outdoor shake table (LHPOST) facility at the University of California, San Diego, for their technical assistance towards the completion of the test program.

Data Availability Statement

The data that support the findings of this study are available from the corresponding author upon reasonable request.

References

1. M. R. Eatherton, P. E. O'Brien, and W. S. Easterling, "Examination of Ductility and Seismic Diaphragm Design Force-Reduction Factors for Steel Deck and Composite Diaphragms," *Journal of Structural Engineering ASCE* 146, no. 11 (2020): 645–651.

2. R. B. Fleischman, J. I. Restrepo, C. J. Naito, R. Sauce, D. Zhang, and M. Schoettler, "Integrated Analytical and Experimental Research to Develop a New Seismic Design Methodology for Precast Concrete Diaphragms," *Earthquake Engineering & Structural Dynamics* 30, no. 5 (2013): 745–763.

3. M. E. Rodriguez, J. I. Restrepo, and J. J. Blandón, "Seismic Design Forces for Rigid Floor Diaphragms in Precast Concrete Building Structures," *Journal of Structural Engineering ASCE* 133, no. 11 (2007): 1604–1615.

4. CERC, *Final Report, Volumes 6: Canterbury Television Building (CTV)* (Canterbury Earthquakes Royal Commission (CERC), 2012).

5. R. B. Fleischman, R. Sause, J. Ricles, et al. "Analytical and Experimental Investigation of Seismic Floor and Roof Collectors in Steel Building Structures," in *Proceedings of the 17th World Conference Earthquake Engineering*, (2020).

6. D. Zhang, R. B. Fleischman, C. J. Naito, and R. Ren, "Experimental Evaluation of Pretopped Precast Diaphragm Critical Flexure Joint Under Seismic Demands," *Journal of Structural Engineering ASCE* 137, no. 10 (2011): 1063–1074.

7. G. Mosqueda, R. Retamales, A. Filiatrault, and A. Reinhorn, "Testing Facility for Experimental Evaluation of Non-Structural Components Under Full-Scale Floor Motions," *Earthquake Spectra* 18 (2009): 387–404.

8. R. Retamales, G. Mosqueda, A. Filiatrault, and A. Reinhorn, "Testing Protocol for Experimental Seismic Qualification of Distributed Nonstructural Systems," *Earthquake Spectra* 27, no. 3 (2011): 835–856.

9. A. K. Chopra, *Dynamics of Structures-Theory and Applications to Earthquake Engineering*. 5th ed. (Prentice Hall, 2017).

10. AISC. *Seismic Design Manual*, 3rd Ed. (AISC, 2018).

11. B. Z. Lin, M. C. Chuang, and K. C. Tsai, "Object-oriented Development and Application of a Nonlinear Structural Analysis Framework," *Advances in Engineering Software* 40, no. 1 (2009): 66–82.

12. Y. F. Dafalias and E. P. Popov, "Plastic Internal Variables Formalism of Cyclic Plasticity," *Journal of Applied Mechanics* 43, no. 4 (1976): 645–651.

13. C. H. Li, M. Reynolds, and C. M. Uang, *Fatigue Testing of CoreBrace Buckling-Restrained Braces*. Report No. TR-18/06 (University of California San Diego, 2021).

14. ASCE. *ASCE/SEI 7–16: Minimum Design Loads for Buildings and Other Structures* (Reston, VA: 2016).

15. R. Sabelli, T. A. Sabol, and W. S Easterling. *Seismic Design of Composite Steel Deck and Concrete-Filled Diaphragms: A guide for Practicing Engineers, NEHRP Seismic Design Technical Brief No. 5 (NIST GCR 11-917-10)* (NEHRP Consultants Joint Venture for the National Institute of Standards and Technology, 2011).

16. J. P. Moehle, J. D. Hooper, D. J. Kelly, and T. Meyer. *Seismic Design of Cast-in-Place Concrete Diaphragms, Chords, and Collectors: A Guide for Practicing Engineers, NEHRP Seismic Design Technical Brief No. 3 (NIST GCR 10-917-4)* (NEHRP Consultants Joint Venture for the National Institute of Standards and Technology, 2010).

17. C. H Li, "Earthquake Simulator Testing and Associated Study on Performance and Design of Seismic Collectors in Steel Buildings," (PhD., diss., University of California San Diego, La Jolla, CA), 2022.

18. S. Torabian, M. R. Eatherton, W. S. Easterling, J. F. Hajjar, and B. W. Schafer, *SDII Building Archetype Design v1.0. Cold-Formed Steel Research Consortium (CFSRC)* (Johns Hopkins University, 2017).

19. O. Ozcelik, J. P. Conte, and J. E. Luco, "Comprehensive Mechanics-based Virtual Model of NHERI@UCSD Shake Table—Uniaxial Configuration and Bare Table Condition," *Earthquake Engineering & Structural Dynamics* 50 (2021): 3288–3310.

20. B. K. Thoen and P. N Laplace. Offline Tuning of Shake Tables. in *Proceedings of 13th World Conference Earthquake Engineering* (2004).